Electronic Supplementary Material (ESI) for Physical Chemistry Chemical Physics.

Tunable Oligo-Histidine Self-assembled Monolayer Junction and Charge Transport by pH Modulated Assembly

Baili Li, ‡ [a] Lixian Tian, ‡ [a] Xuehao He, [a] Xuan Ji, [a] Hira Khalid, [a] Chong Yue, [b] Qinggang Liu, [b] Xi Yu, [a] Shengbin Lei,* [a] and Wenping Hu* [a]*

[a] Department of Chemistry, Tianjin Key Laboratory of Molecular Optoelectronic Sciences, School of Science, Tianjin University and Collaborative Innovation Center of Chemical Science and Engineering (Tianjin), Tianjin, 300072, China

[b] State Key Laboratory of Precision Measurement Technology and Instruments, School of Precision Instrument and Opto-Electronics Engineering, Tianjin University, Tianjin 300072, China

KEYWORDS: Charge Transport, Molecular Junction, Peptide Conformation, Self-Assembled Monolayer, Series Tunneling

Supporting Information

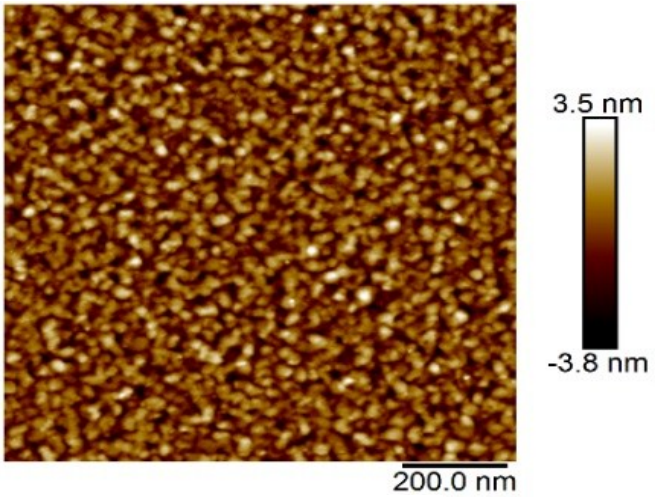

Figure S1. AFM height image of bare gold substrate.

1. Characterization of 7-His solution and SAMs.

The surface topography of bare gold substrate was characterized using AFM tapping mode. Figure S1 shows the height image of bare gold substrate, in which the grains of gold particles are illustrated. The roughness of the gold substrates for SAM growth is about 1.2nm.

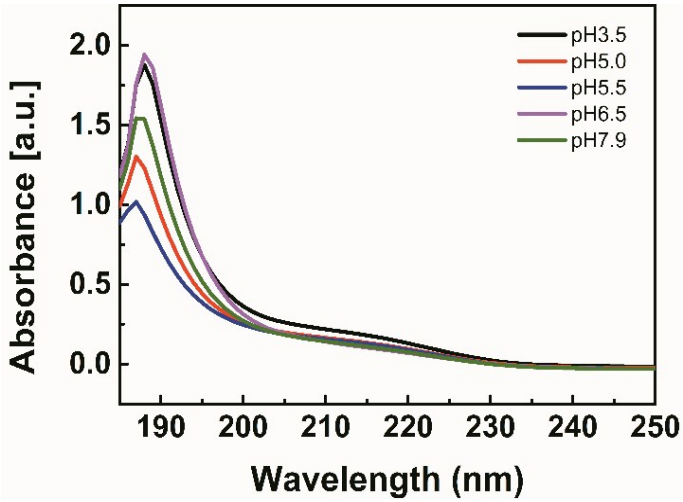

Figure S2. UV absorption spectra of 7-His solutions with different pH values.

The UV absorption was measured to calculate optical energy bandgap of 7-His in different pH solutions, see UV spectra of 7-His solution of varied pH in Figure S2.

The IR bands around 1110 and 1090 cm^{-1}, which belong to imidazole ring =C-N stretching vibrations coupled to the corresponding =C-H in-plane deformation, can be used as marker to detect the protonation/deprotonation state of 7-His in solutions.[1, 2] The band around 1090 cm^{-1} represents IR mode when two nitrogen atoms in the imidazole are protonated while band around 1110 cm^{-1} indicates the imidazole is in neutral τ-tautomer form with only one nitrogen protonated. Figure 3a in the paper shows attenuated total reflection-Infra red spectra (ATR-IR) of 7-His solutions of pH 3.5, pH 5.5 and pH 7.9. Both IR bands of 1110 and 1090 cm^{-1} can be observed for 7-His solutions of tested pH values, which indicates imidazole groups in 7-His presents both positively charged and neutral tautomer forms. The decrease in peak intensity around 1090 cm^{-1} together with increase trend in peak intensity around 1110 cm^{-1} proves the decrease in number of protonated nitrogen atoms in imidazole group upon higher solution pH.

To investigate the conformational change of 7-His in solutions of varied pH we measured UV circular dichroism (CD) and found that 7-His presents random coil secondary structure in solutions with pH ranging from 3.5 to 7.9, a positive peak around 220nm and a negative peak around 200nm. Peak shift at around 220nm together with intensity change at both 195nm and 220nm occurs upon

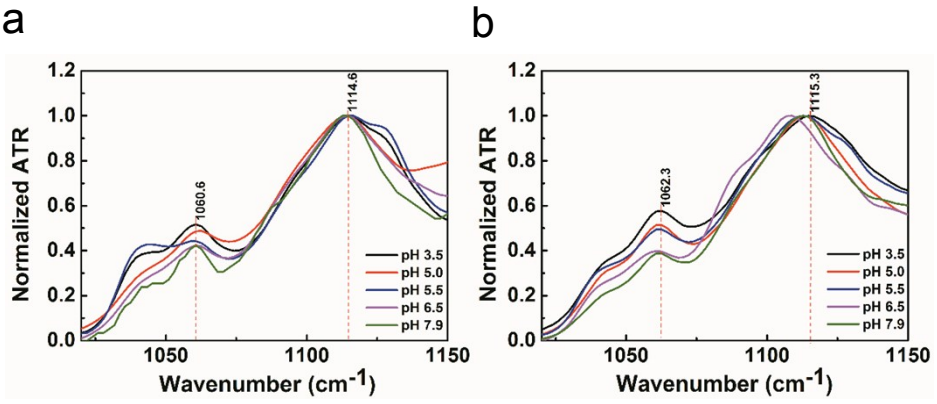

Figure S3. ATR-IR spectra of (a) 7-His SAMs post washed with neutral solvent and (b) 7-His SAMs post washed with corresponding acidic solvents.

increase of solution pH, which indicates a change in the conformation with different solution pH[3-5].

Attenuated total reflection-Infra red spectrum (ATR-IR) was used to characterize the 7-His monolayer with a Bruker 70 with Ge ATR accessory. We focus on the peaks around 1110 cm^{-1}, which belong to the coupled skeletal stretching and bending modes of C-N, C-C, N-H and C-H of imidazole, and are sensitive to the protonation state of the imidazole. As can be seen in Figure S3, peaks around 1110 cm^{-1} of 7-His SAMs with neutral post rinsing exhibits no significant change which indicates similar protonation state.[1] The relative intensity of peak 1114 cm^{-1} (skeletal stretching and bending modes) and 1060 cm^{-1} (side chain C-N stretching modes) can also be used as a marker of protonation state. [2] The relative intensity of 1114 cm^{-1} and 1060 cm^{-1} fluctuates slightly in neutral post rinsed SAMs while a clear increase trend exists in SAMs of acid post rinsing (for acid post rinsing HCl was added to water to achieve desired pH. HCl was purchased from Kermel Co., Ltd.) with increasing pH.

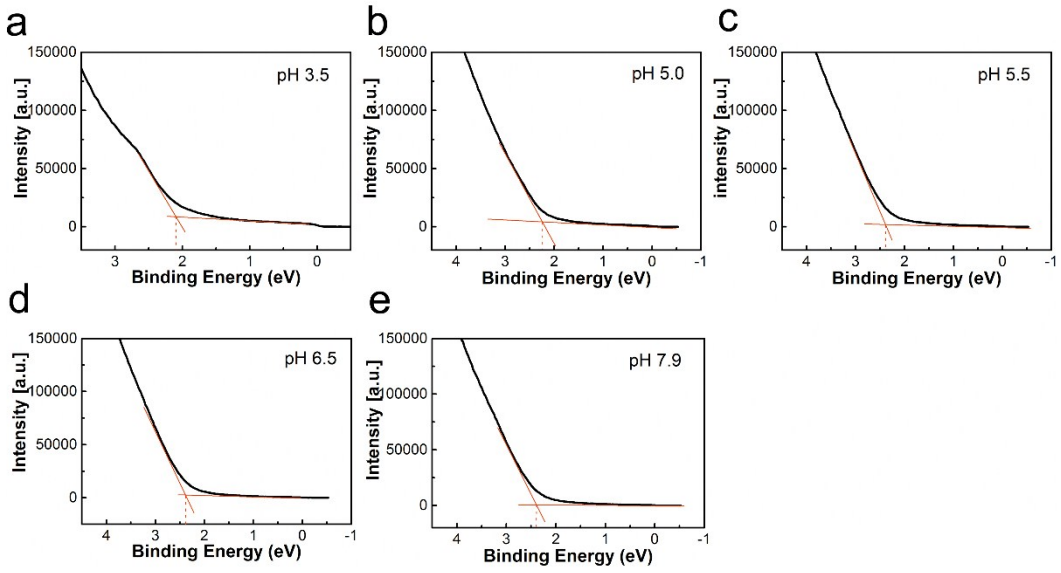

Figure S4. UPS spectra of 7-His monolayer on Au prepared from different pH value solutions and rinsed using neutral solution.

UPS of 7-His SAMs on gold substrates that were grown from different solution pH from 3.5 to 7.9 was measured to obtain information of electronic states of 7-His SAMs, see Figure S4.

2. 7-His Junction I-V Characterization.

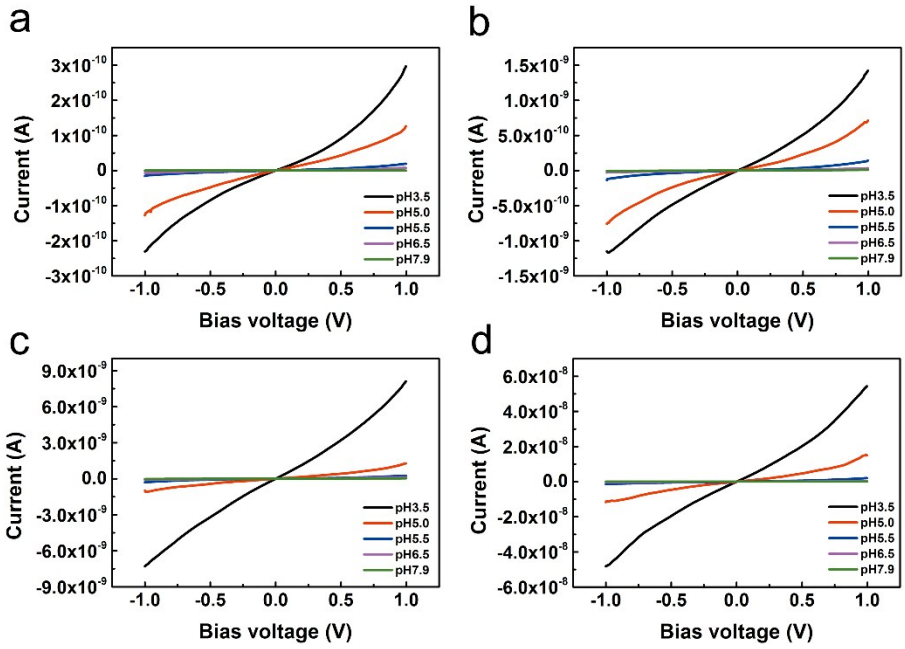

Figure S5. I-V curves of 7-His SAMs with different thickness measured from CP-AFM under (a) 4 nN, (b) 8 nN, (c) 12 nN and (d) 20 nN.

Figure S5 shows I-V curves measured under 4 nN, 8 nN, 12 nN and 20 nN, respectively. Linear current-voltage relation at low bias voltage and nonlinear current-voltage relation at high bias voltage can be observed.

3. Single-level Model Fitting.

The current-voltage relation is:

$$I \cong n\frac{2e}{h}\Gamma^2\frac{eV}{(\varphi + (0.5-\alpha)eV)^2 - (eV/2)^2} \quad \text{(S1)}$$

We first simplified Eq S1 as following:

$$y \cong at^2 \frac{x}{(b+cx)^2 - (x/2)^2} \quad \text{(S2)}$$

$$a = n\frac{2e}{h},\ b = \varphi,\ c = (0.5 - \alpha),\ t = \Gamma$$

The effective number of molecules in the junction is taken as 100 considering the AFM tip radius. The single-level model fitted parameters and fitting curves of I-V curves under 8 nN are illustrated in Table S1 and Figure S6 respectively.

Table S1. Values of transition voltage V_t and obtained energy offset ε_h, coupling strength Γ and HOMO energy offset φ from single-level model fitting.

SAM pH	3.5	5.0	5.5	6.5	7.9
V_t (V)	0.90/-0.95	0.83/-0.89	0.81/-0.92	-	-
ε_h(eV)	0.80	0.74	0.75	-	-
Γ (meV)	3.65±0.33	1.86±0.21	0.71±0.074	0.50±0.077	0.21±0.031
φ (eV)	0.86±0.003	0.70±0.003	0.69±0.002	0.74±0.006	0.72±0.005

It has been reported by Frisbie et al. that transition voltage V_t has a correlation with energy offset of the molecular junctions.[6] The correlation can be expressed as:

$$e^{V_t} = 2^{\varepsilon_h/\sqrt{3}} \quad \text{(S3)}$$

We have plotted ln(I/V²) over 1/V and extracted V_t and ε_h from TVS plots. For 7-His SAMs prepared from solution of pH 3.5, 5.0 and 5.5 we found good correlation between TVS extracted

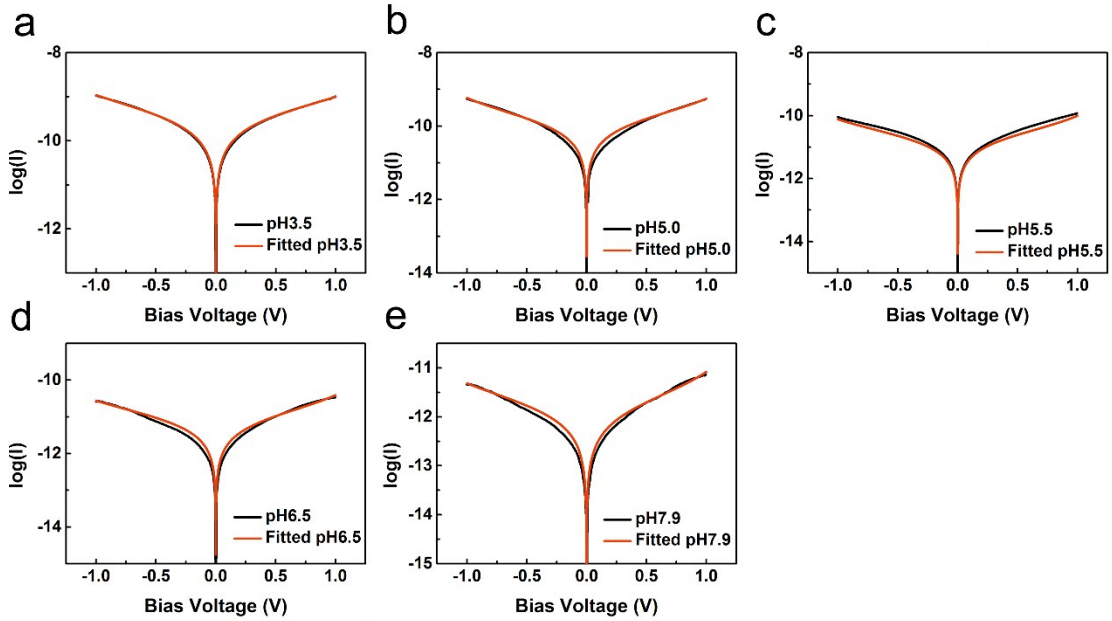

Figure S6. Single-level model fitted and experimental log(I)-V curves measured under 8 nN for 7-His prepared from solution with (a) pH 3.5, (b) pH 5.0, (c) pH 5.5, (d) pH 6.5, (e) pH 7.9.

ε_h and single level fitted energy offset φ, while for 7-His SAMs prepared from solution of pH 6.5 and 7.9 it is not able to obtain V_t from the plot, see Figure S7 and Table 1.

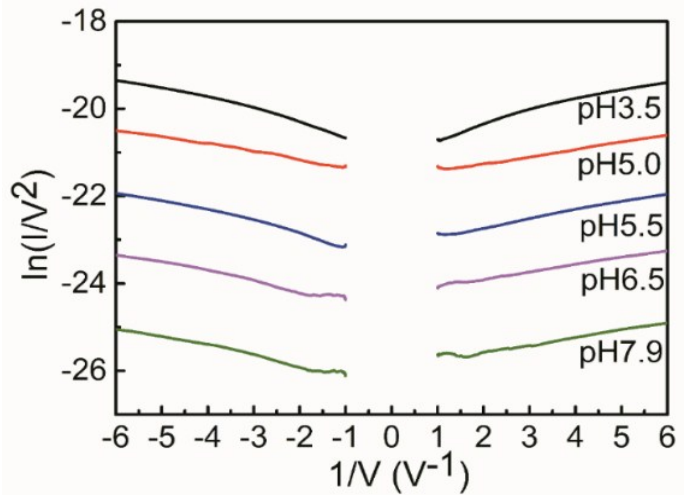

Figure S7. Transition voltage (ln(I/V²) vs 1/V) spectra obtained under 8 nN for 7-His prepared from solution with pH 3.5, pH 5.0, pH 5.5, pH 6.5, pH 7.9.

4. Multi-level Model Fitting.

Multi-level model incorporates details of molecular structure into electron tunneling through the junction. This model considers the tunneling of electron across a single molecule in a metal-molecule-metal junction under certain bias voltage. The tunneling barrier is composed with multi-energy levels corresponds to the molecular electronic states.[7]

$$I(V) = \frac{2e}{\pi\hbar(1-2N)t}\Delta_0^2 n\left\{\left(\frac{e\varphi + (\frac{eV}{2})}{t}\right)^{1-2N} - \left(\frac{e\varphi - (\frac{eV}{2})}{t}\right)^{1-2N}\right\} \quad \text{(S4)}$$

where n is the number of molecules per unit area in the junction, Δ_0 is spectral density of either of the two electrodes at zero bias, N is the number of energy sites in the molecular bridge and t is the transfer integral between them, and φ is the difference between the Fermi level of the electrode and the energy of each site in the molecule.[8]

The fitting of Eq S4 to the experimental I-V curves from CP-AFM of 7-His junctions with different width has been done with following strategies considering the mathematical difficulties as mentioned in the main text.

We first simplified Eq S4 as following:

$$y = \frac{a}{tc}\left\{\left(\frac{b + x/2}{t}\right)^c - \left(\frac{b - x/2}{t}\right)^c\right\} \quad \text{(S5)}$$

$$a = \frac{2e}{\pi\hbar}\Delta_0^2 n, \quad b = e\varphi, \; c = 1 - 2N.$$

and the value of n and Δ_0^2 were taken to be 100 and 5×10^{-6} eV^2,[7-9] respectively. To obtain valid fitting it is crucial that initial values of the tunneling parameters used in the simulation should be close to the physically reasonable values. UPS data suggests good initial value for φ, while SAM thickness provides suitable initial value for N. In order to assume a possible initial value for t,

following the exponential dependence of the current on the width of the junction *d* based on this model, which is $I \propto e^{-\beta d}$ with:

$$\beta = \frac{2}{a} ln\left(\frac{e\varphi - \frac{eV}{2}}{|t|}\right) \quad \text{(S6)}$$

where *a* is the length between two energy sites and we took *a* to be 3 Å by assuming the energy sites here are the imidazole side groups of histidine and the inter-molecular distance is the Van der Waals distance. With decay constant β extracted from experimental data at 0.2 V, possible initial value for t can be calculated to be about 0.9. Using these initial values, we run the test fitting with *c*, φ and *t* as free parameters to obtain a closer value. In order to further reduce the mathematical difficulty of the fitting algorithm, we have fixed *t* at 0.84 in the fitting process and the fitting with free parameters of *c* and φ obtained well fitted and physical reasonable results.

Fitted tunneling parameters and fitting curves are shown in Table S2 and Figure S8 below.

Table S2. Values of *c*, the number of sites *N*, HOMO energy offset φ and attenuation factor β from multi-level model fitting and direct UPS data.

SAM pH	3.5	5.0	5.5	6.5	7.9
c	-4.06±0.04	-5.21±0.06	-7.59±0.06	-9.64±0.14	-11.10±0.17
N	2.53±0.02	3.11±0.03	4.29±0.03	5.32±0.07	6.05±0.09
φ (eV)	1.98±0.01	1.93±0.01	1.97±0.01	1.87±0.01	1.97±0.02
UPS (eV)	2.1	2.2	2.4	2.4	2.4
β ($Å^{-1}$)	0.54	0.52	0.53	0.50	0.53

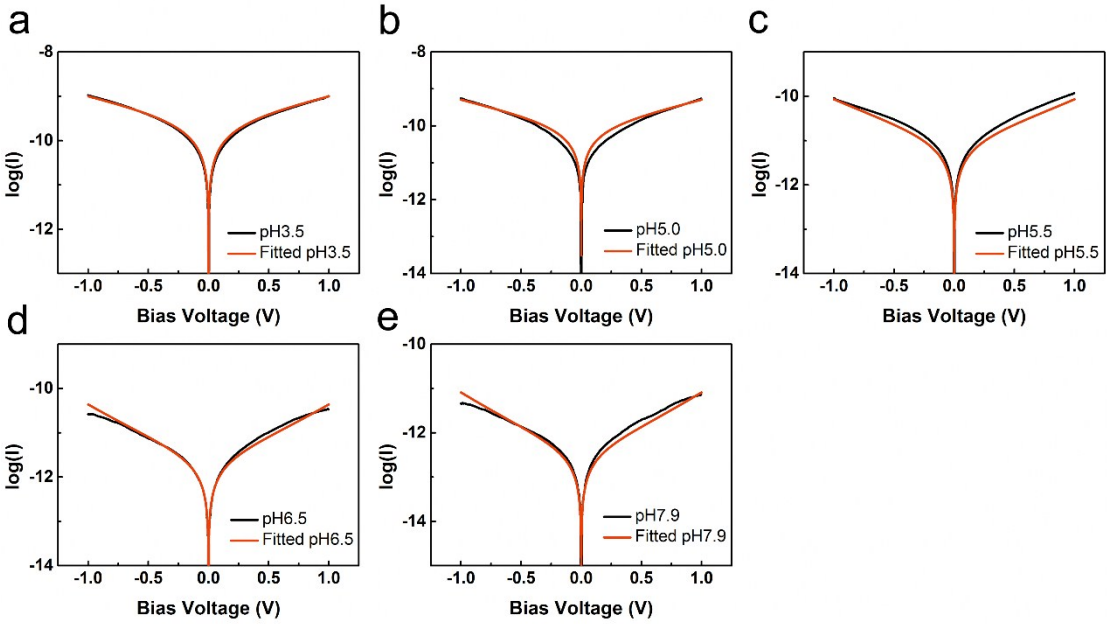

Figure S8. Multi-level model fitted and experimental log(I)-V curves measured under 8 nN for 7-His prepared from solution with (a) pH 3.5, (b) pH 5.0, (c) pH 5.5, (d) pH 6.5, (e) pH 7.9. Black lines show experimental log(I)-V data and red lines show fitted data.

The number of energy sites N exhibits physically reasonable values and shows a linear increase as SAM thickness increases. The energy difference between sites and electrode Fermi level remained nearly constant with a small fluctuation. The values of φ obtained from multi-level model are much closer to UPS experimental data as compared with the energy-offset fitted from single-level model, which can be explained by the over simplification in single-level model to consider oligopeptide as a single energy level. The calculated β values from fitted parameters in Eq S5 agrees well with β=0.52±0.07 $Å^{-1}$ of experimental extracted value. These results show that multi-level model is suitable to generate physically reasonable tunneling parameters of oligopeptide junctions.

We found that the exponential decrease of the coupling to the electrodes (Γ) in single-level fitted is a typical mathematical "artifact" when single-level model is used to fit the I-V data of molecular junctions baring multi-states series tunneling.

To demonstrate this point, we first generated I-V data using the multi-state series tunneling model with varied number of sites (N=3, 4, 5, 6, 7) (number of molecules in the junction is fixed at n=100, energy offset φ=2, and t=0.8). Then, we used single-level model to fit these generated I-V data and good fitting was found (as shown in Figure S9). The coupling (Γ) obtained by single-level model fitting at N = 3, 4, 5, 6, 7 is illustrated in Figure S10 and exponential decrease of coupling with increasing number of energy sites can be found.

Therefore, the exponential decrease in coupling fitted from single-level model results from the change in number of energy sites in molecular junctions consisting multi-states. Underline origin for this phenomenon from physical model point of view is not clear yet and deserves further study.

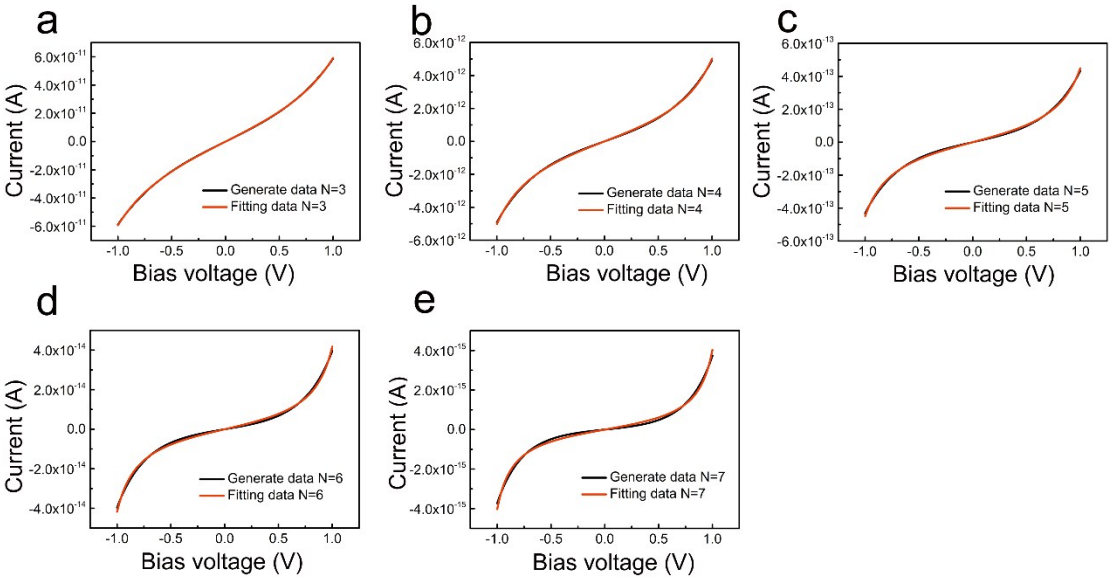

Figure S9. Single-level model fitting using data generated by multi-level model. a-e show the fitting result and I-V data generated with number of energy sites N equals 3, 4, 5, 6, 7, respectively.

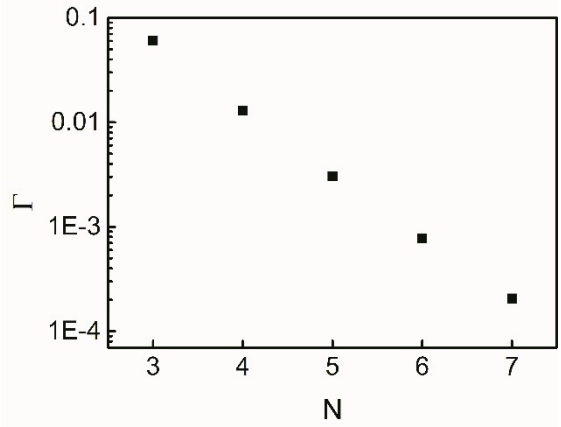

Figure S10. Exponential decrease of single-level model fitted coupling Γ with increase of number of energy sites N.

5. Molecular Dynamics Model and Simulation Details.

In order to understand the conformations of oligo-histidine (7-His) with varied protonated structures corresponding to different pH situations, all-atomic molecular dynamic was further carried out. All 7-histidine models were constructed with the ionizable COO- and NH3+ groups at the C-terminal and N-terminal respectively. For a histidine unit, three kinds of structures corresponding to neutral histidine HISD with N_δ protonated HISD, neutral histidine with N_ϵ protonated HISE, and positive histidine with both N_δ and N_ϵ protonated HISP, can been considered. Neutral histidine (HISD or HISE) exists in the solution with a medium pH value (6~8). Positive histidine (HISP) exists in the solution with a low pH (3~5). In our simulation, four 7-histidine models (M1, M2, M3 and M4) were constructed with the different sequences of histidine. M1 consists of 7 HISD. M2 is with 7 HISE and M3 is with 3 HISD and 4 HISE (EDDEEDE). M4 is with 7 HISP. The initial conformations of M1, M2, M3 and M4 are shown in Figure S11. All simulations were performed with GROMACS (version 2018.6) [10], using OPLS/AA[11] force field of

histidine model and TIP3P[12] for water model, respectively. In each simulation, the water cube containing a 7-His and ~9000 water was employed. For the positive histidine (HISP in M4), Cl^- counterions were added to keep the charge neutrality of system. In simulation, periodic boundary condition was used and the lincs algorithm[13,14] was applied to all-bonds to allow a 2 fs time step with a leapfrog integrator. The coulomb interactions were calculated with PME method[15] where the real-space cutoff was set as 10 Å and the grid spacing was 1.6 Å. The range of van der Waals interaction was set as 10 Å. The molecular conformation was saved every 20000 time steps. Prior to the production runs, the molecular configurations were energy minimized with steepest descent. After that, the molecular dynamics was equilibrated for 800 ns in the NPT ensemble at 1 bar (Parrinello−Rahman barostat[16] with τP = 2 ps) and at 300 K (Nosé−Hoover thermostat[17,18] with τT = 0.1ps). The equilibrium conformations were extracted from the final 400ns for analysis. The snapshot conformations indicate that 7-His conformation changes all the time without well-defined structure. (as shown in Figure S12) The revolution of gyration radius for M1, M2, M3 and M4 is shown in Figure S13 and the average value of gyration radius for M1, M2, M3 and M4 were calculated and summarized. (Table S3). It is illustrated that the average gyration radii of M1, M2, M3 and M4 for 7-His oligomer are similar and the difference of chain extension is small.

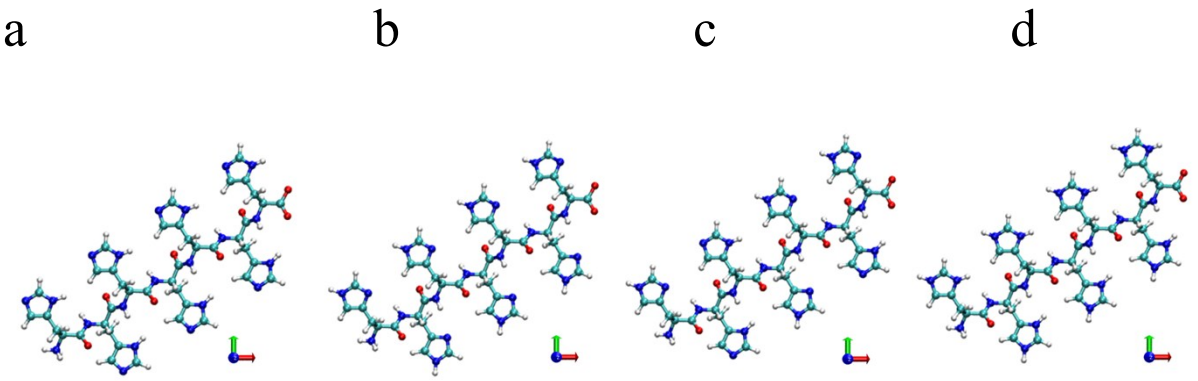

Figure S11. The initial conformations of oligo-histidine (7-His). a: M1 with 7 HISD; b: M2 with 7HISE; c: M3 with 3 HISD and 4 HISE; d: M4 with 7 HISP.

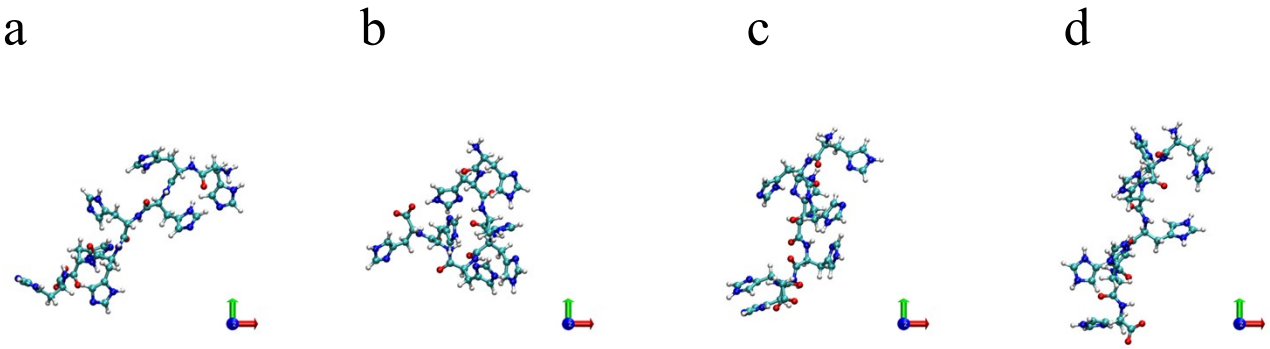

Figure S12. The snapshot conformations of oligo-histidine (7-His) at equilibrium state. a: M1 with 7 HISD; b: M2 with 7HISE; c: M3 with 3 HISD and 4 HISE; d: M4 with 7 HISP.

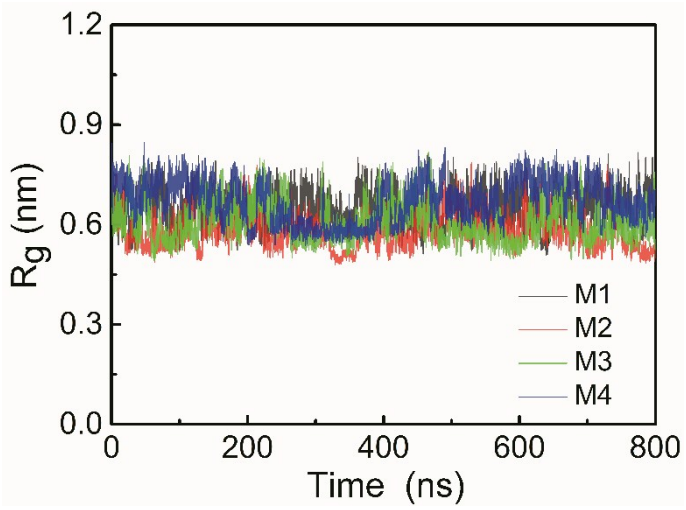

Figure S13. The gyration radius evolutions of M1, M2, M3 and M4 with time. M1: with 7 HISD; M2: with 7HISE; M3: with 3 HISD and 4 HISE; M4: with 7 HISP.

Table S3. The average gyration radius $\bar{R}g$ of oligo-histidine (7-His).

Oligo-histidine	$\bar{R}g$ (nm)
M1 (7 HISD)	0.65±0.05
M2 (7 HISE)	0.58±0.05
M3(3 HISD + 4 HISE)	0.60±0.05
M4(7 HISP)	0.69±0.05

6. Electronic structure calculations.

The electronic-structure calculations were carried out by using the Gaussian 09 program.[19] Since the MD simulation revealed that the peptides take on random ill-defined structure with ever-lasting conformational change, geometric optimization of the MPA-7His will be too expensive. We therefore studied MPA-Histidine (MPA-His), MPA-di-histidine (MPA-2His) and MPA-tri-histidine (MPA-3His) as smaller representatives of MPA-7His. Geometries of MPA-His, MPA-2His and MPA-3His were optimized respectively by using DFT method, with B3LYP hybrid functionals and 3-21G basis set. After that, we performed further optimization and frequency calculations by changing the basis set into 6-31+G(d). The structures obtained present no imaginary vibrational frequencies, indicating that the obtained structures are at the minima of the potential energy surface. We then studied the electronic structure of the peptides at the optimized geometry. As can be seen in Figure S14, the HOMOs of the three peptides are mainly localized on imidazole rings of histidine. (Although the orbital of the MPA thiol group is also close to the HOMO of the peptides and become part of the HOMOs of the molecule, it only resides at the end of the molecular chain and played smaller role as the peptides become longer.) Therefore, the

HOMO of 7-His should also locate on the conjugated imidazole ring, similar to MPA-2His and MPA-3His.

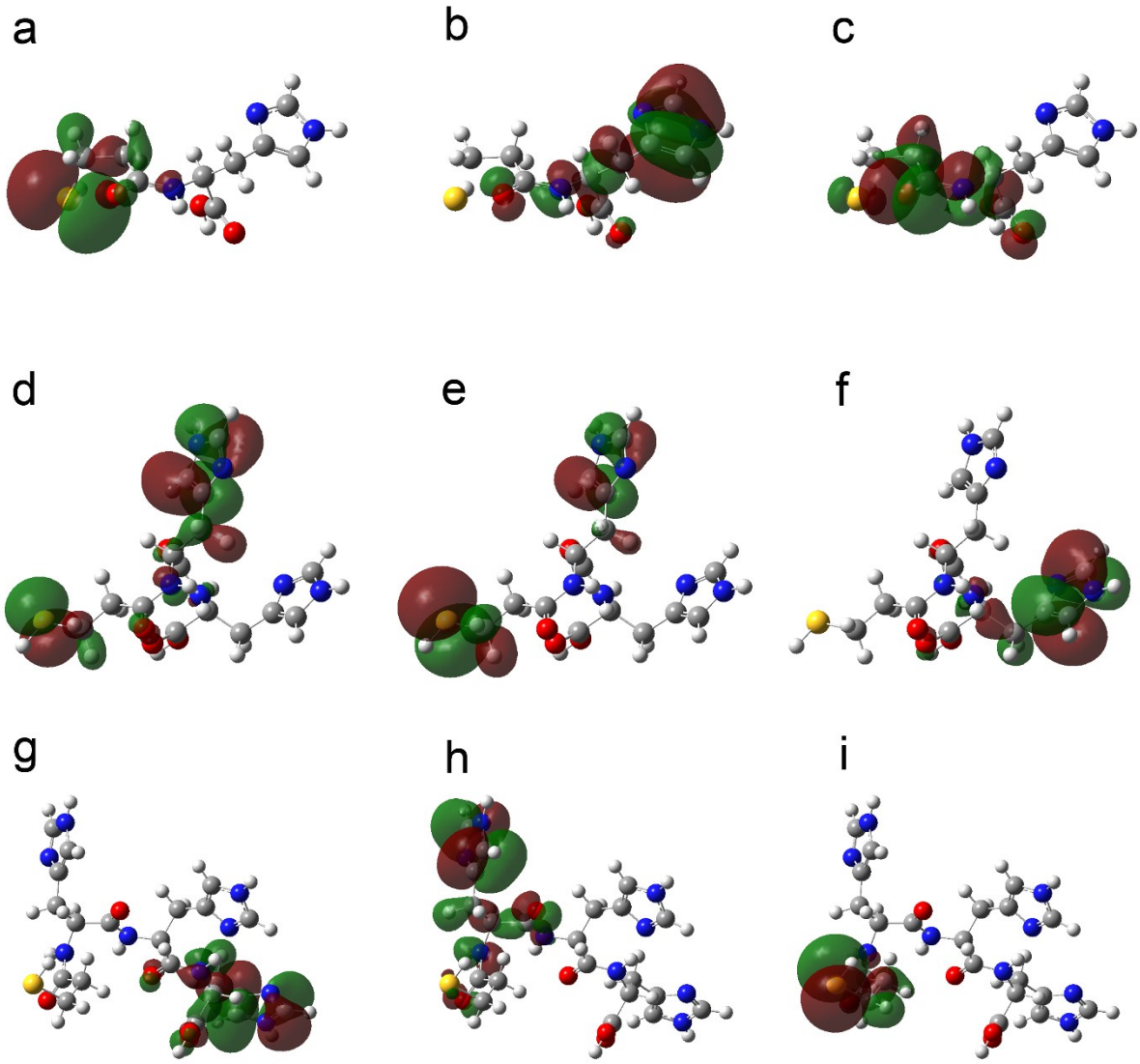

Figure S14. The DFT calculated electronic structure of MPA-His (a: HOMO, b: HOMO-1, c: HOMO-2), MPA-2His (d: HOMO, e: HOMO-1, f: HOMO-2) and MPA-3His (g: HOMO, h: HOMO-1, i: HOMO-2).

REFERENCES

(1) K. B. Alici, I. F. Gallardo, *SCI. REP*. 2013, **3**, 2956.

(2) J. G. Mesu, T. Visser, F. Soulimani, B. M. Weckhuysen, *Vib. Spectrosc.* 2005, **39**, 114.

(3) C. Zerfaß, G. W. Buchko, W. J. Shaw, S. Hobe, H. Paulsen, *PROTEINS*. 2017, **85**, 2111.

(4) J. Khandogin, J. Chen, C. L. Brooks, *Proc. Natl. Acad. Sci.* 2006, **103**, 18546.

(5) R. P. Bonomo, G. Impellizzeri, G. Pappalardo, E. Rizzarelli, G. Tabbì, *CHEM-EUR J.* 2000, **6**, 4195.

(6) Z. Xie, I. Bâldea, C. E. Smith, Y. Wu, C. D. Frisbie, *ACS Nano*. 2015, **9**, 8022.

(7) V. Mujica, M. A. Ratner, *Chem. Phys*. 2001, **264**, 365.

(8). R. E. Holmlin, R. F. Ismagilov, R. Haag, V. Mujica, M. A. Ratner, M. A. Rampi, G. M. Whitesides, *Angew. Chem., Int. Ed.* 2001, **40**, 2316.

(9) R. Farzadi, H. M. Moghaddam, A. Bahari, *Indian. J. Phys.* 2014, **88**, 667.

(10) D. Van der Spoel, E. Lindahl, B. Hess, G. Groenhof, A. E. Mark and H. J. C. Berendsen, *J. Comput. Chem*., 2005, **26**, 170.

(11) W. L. Jorgensen, J. D. Madura and C. J. Swenson, *J. Am. Chem. Soc*, 1984, **106**, 6638.

(12) W. L. Jorgensen, J. Chandrasekhar, J. D. Madura, R. W. Impey and M. L. Klein, *J. Chem. Phys.*, 1983, **79**, 926.

(13) B. Hess, H. Bekker, H. J. C. Berendsen and J. G. E. M. Fraaije, *J. Comput. Chem*., 1997, **18**, 1463.

(14) B. Hess, J. Chem. *Theory Comput*., 2008, **4**, 116.

(15) U. Essmann, L. Perera, M. L. Berkowitz, T. Darden, H. Lee and L. G. Pedersen, *J. Chem. Phys.*, 1995, **103**, 8577.

(16) M. Parrinello and A. Rahman, *J. Appl. Phys.*, 1981, **52**, 7182.

(17) S. Nosé, *J. Chem. Phys.*, 1984, **81**, 511.

(18) W. G. Hoover, *Phys. Rev. A.*, 1985, **31**, 1695.

(19) Gaussian 09, M. J. Frisch, G. W. Trucks, H. B. Schlegel, G. E. Scuseria, M. A. Robb, J. R. Cheeseman, G. Scalmani, V. Barone, G. A. Petersson, H. Nakatsuji, X. Li, M. Caricato, A. Marenich, J. Bloino, B. G. Janesko, R. Gomperts, B. Mennucci, H. P. Hratchian, J. V. Ortiz, A. F. Izmaylov, J. L. Sonnenberg, D. Williams-Young, F. Ding, F. Lipparini, F. Egidi, J. Goings, B. Peng, A. Petrone, T. Henderson, D. Ranasinghe, V. G. Zakrzewski, J. Gao, N. Rega, G. Zheng, W. Liang, M. Hada, M. Ehara, K. Toyota, R. Fukuda, J. Hasegawa, M. Ishida, T. Nakajima, Y. Honda, O. Kitao, H. Nakai, T. Vreven, K. Throssell, J. A. Montgomery, Jr., J. E. Peralta, F. Ogliaro, M. Bearpark, J. J. Heyd, E. Brothers, K. N. Kudin, V. N. Staroverov, T. Keith, R. Kobayashi, J. Normand, K. Raghavachari, A. Rendell, J. C. Burant, S. S. Iyengar, J. Tomasi, M. Cossi, J. M. Millam, M. Klene, C. Adamo, R. Cammi, J. W. Ochterski, R. L. Martin, K. Morokuma, O. Farkas, J. B. Foresman, and D. J. Fox, Gaussian, Inc., Wallingford CT, 2016.